Nonclassical Photon Number Distribution in a Superconducting Cavity under a Squeezed Drive

S. Kono, Y. Masuyama, T. Ishikawa, Y. Tabuchi, R. Yamazaki, K. Usami, K. Koshino, and Y. Nakamura

Phys. Rev. Lett. **119**, 023602 — Published 13 July 2017

DOI: 10.1103/PhysRevLett.119.023602

Nonclassical photon number distribution in a superconducting cavity under a squeezed drive

S. Kono[1], Y. Masuyama[1], T. Ishikawa[1], Y. Tabuchi[1], R. Yamazaki[1], K. Usami[1], K. Koshino[2], and Y. Nakamura[1,3]
[1]*Research Center for Advanced Science and Technology (RCAST), The University of Tokyo, Meguro-ku, Tokyo 153-8904, Japan*
[2]*College of Liberal Arts and Sciences, Tokyo Medical and Dental University, Ichikawa, Chiba 272-0827, Japan and*
[3]*Center for Emergnent Matter Science (CEMS), RIKEN, Wako, Saitama 351-0198, Japan*
(Dated: June 7, 2017)

A superconducting qubit in the strong dispersive regime of circuit quantum electrodynamics is a powerful probe for microwave photons in a cavity mode. In this regime, a qubit excitation spectrum is split into multiple peaks, with each peak corresponding to an individual photon number in the cavity (discrete ac Stark shift). Here, we measure the qubit spectrum in a cavity that is driven continuously with a squeezed vacuum generated by a Josephson parametric amplifier. By fitting the obtained spectrum with a model which takes into account the finite qubit excitation power, we determine the photon number distribution, which reveals an even-odd photon number oscillation and quantitatively fulfills Klyshko's criterion for nonclassicality.

Advancement of the superconducting quantum circuit technologies [1] and the concept of circuit quantum electrodynamics (QED) [2] have led to the emergence of microwave quantum optics, enabling us to generate and characterize nonclassical states of electromagnetic fields in the microwave domain.

A squeezed vacuum is one of the most widely studied nonclassical states as a resource in quantum technologies, such as computation, communication and metrology [3]. In microwave quantum optics, a squeezed vacuum is conveniently generated by degenerated parametric down conversion in a Josephson parametric amplifier (JPA) based on the nonlinearity of Josephson junctions [4, 5]. Characterizations of such states propagating in a waveguide have been realized by measuring the quadrature amplitudes with a homodyne technique with the aid of a JPA [6] or a cryogenic HEMT amplifier [7, 8]. JPAs and related circuits are also used to generate and characterize two-mode squeezing in spatially or spectrally separated propagating modes [9–13]. More recently, it has been shown that a squeezed vacuum injected in a cavity induces nontrivial effects to the relaxations of a qubit [14, 15] and a spin ensemble [16]. In the Fock basis, on the other hand, a squeezed vacuum displays another feature of the nonclassicality, i.e., the photon number distribution composed of only even photon numbers [17]. In the optical domain, direct observations of photon number distribution using a photon-number-resolving detector were reported [18, 19]. In the microwave domain, however, because of the smallness of the energy of a single photon, photon counting in a propagating mode is still a challenging task, while a few realizations of microwave single-photon detectors have been reported [20–22].

Here, we report the measurement of the photon number distribution of a squeezed vacuum continuously injected into a cavity containing a superconducting qubit. In the strong dispersive regime of the circuit-QED architecture, the spectrum of a superconducting qubit is split into multiple peaks, with each peak corresponding to a different photon number in a cavity [23, 24]. Furthermore, it is known that the area ratio of the peaks obeys the photon number distribution in the cavity [25]. In practice, however, we find the effect of the finite power of the qubit drive field, which gives rise to a discrepancy between the observed peak area ratio and the actual photon number distribution. At the same time, it turns out that the qubit drive actually enhances the signal-to-noise ratio of the photon number peaks in the qubit spectrum. By fitting the obtained spectrum with a model which takes into account the effect, we determine the actual photon number distribution. The photon number distribution confirms its nonclassicality by Klyshko's criterion, quantitatively indicating an even-odd photon number oscillation [26]. This is a steady-state realization and characterization of a nonclassical photon number distribution in a cavity which is continuously driven by a squeezed vacuum. Owing to the input-output relation [27], the photon number distribution in the cavity can be interpreted as that of the injected microwave state in a propagating mode. It is in stark contrast with the dynamical generations and characterizations of nonclassical states (e.g., cat states) in a cavity [28, 29].

We use a circuit-QED system in the strong dispersive regime, where a transmon qubit is mounted at the center of a three-dimensional superconducting cavity as shown schematically in Fig. 1(a). Setting $\hbar = 1$, the qubit-cavity coupled system is described by the Hamiltonian

$$\mathcal{H} = \omega_{\rm c} a^\dagger a + \frac{\omega_{\rm q}}{2}\sigma_z - \chi a^\dagger a \sigma_z, \tag{1}$$

where $a^\dagger(a)$ is the creation (annihilation) operator of the cavity mode, σ_z is the Pauli operator of the transmon qubit, $\omega_{\rm c}/2\pi = 10.4005$ GHz is the cavity resonant frequency, $\omega_{\rm q}/2\pi = 8.7941$ GHz is the qubit resonant frequency, and $\chi/2\pi = 3.9$ MHz is the dispersive shift. Note that the Hamiltonian is truncated to the subspace of the

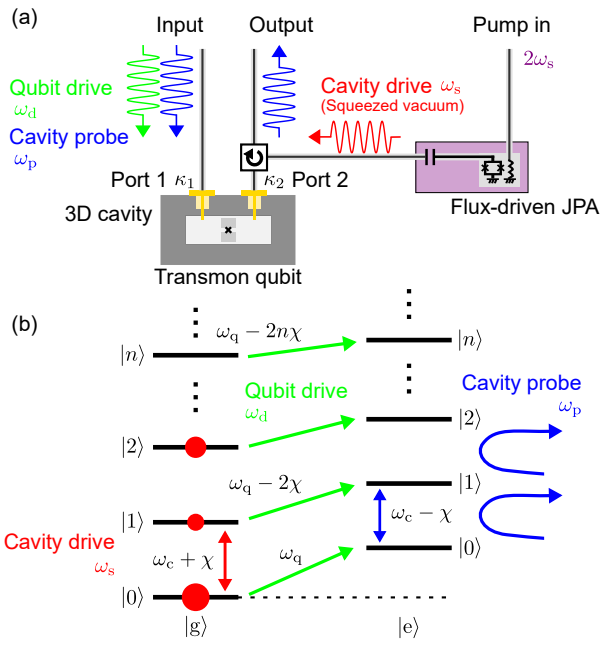

FIG. 1. (a) Schematic of the experimental setup with squeezed vacuum injection. A squeezed vacuum generated by a flux-driven Josephson parametric amplifier (JPA), as a cavity drive field at ω_s, is injected into the cavity from port 2. The cavity probe field at ω_p and the qubit drive field at ω_d are input from port 1, and the transmission of the cavity probe field is measured. The cavity is designed to have asymmetric external coupling rates of $\kappa_2 \approx 100 \times \kappa_1$. For the thermal- and coherent-state injections, the connection to the JPA is switched to a heavily attenuated microwave line connected to the respective sources at room temperature. (b) Energy levels of a dispersively coupled qubit-cavity system. $|g\rangle$ and $|e\rangle$ label the ground and the first exited states of the transmon qubit, and $|n\rangle$ $(n = 0, 1, 2, \cdots)$ indicates the photon number states of the cavity. The cavity drive field generates the steady-state photon number distribution in the cavity (red dots).

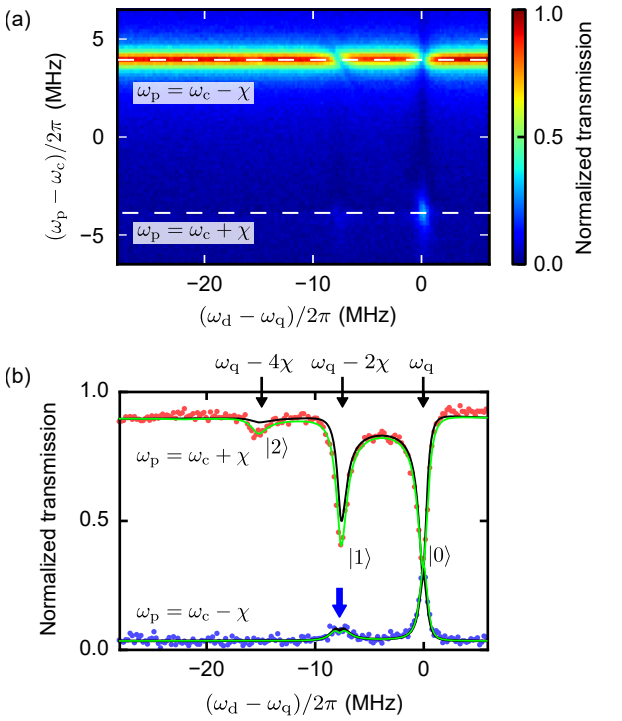

FIG. 2. (a) Cavity transmission as a function of the qubit drive frequency ω_d and the cavity probe frequency ω_p. The transmission is normalized by the maximum peak value. White dashed lines indicate $\omega_p = \omega_c \pm \chi$. (b) Cross sections of (a) at $\omega_p = \omega_c \pm \chi$ (red and blue dots, respectively). Green lines represent the rigorous numerical results in which the finite cavity probe power is fully incorporated, whereas the black lines represent the numerical results within the linear response to the cavity probe field, which corresponds to the weak power limit of the cavity probe field. The splitting of the single-photon peak, which is observed for $\omega_p = \omega_c - \chi$ (blue arrow), is understood as the Autler-Townes effect of the qubit, driven strongly at $\omega_d = \omega_q - 2\chi$ (see [30] for the details).

ground state $|g\rangle$ and the first excited state $|e\rangle$ of the transmon qubit; the higher excited states of the qubit are not populated in the experiment below. The total decay rate of the cavity is $\kappa/2\pi = 0.5$ MHz, the relaxation time of the qubit is $T_1 = 5.5$ μs, and the dephasing time of the qubit is $T_2^* = 4.5$ μs, determined respectively from independent measurements. As shown in Fig. 1(b), the dispersive interaction produces both, the qubit-state-dependent shift of the cavity resonant frequency and the photon-number-dependent light shift of the qubit resonant frequency (discrete ac Stark shift).

In our experiment, three inputs of continuous microwaves are used: a cavity drive, a qubit drive and a cavity probe (see Fig. 1). The cavity drive field, whose frequency ω_s is fixed at the cavity resonant frequency for the qubit in the ground state, $\omega_c + \chi$, is injected to the cavity to generate the steady-state photon number distribution. The qubit drive field is applied to the qubit whose excitation probability depends on the photon number distribution in the cavity. The cavity probe field, whose frequency ω_p is fixed around the cavity resonant frequency, is used to probe the transmission of the cavity depending on the the qubit excitation probability. By measuring the cavity transmission as a function of the qubit drive frequency ω_d, we can observe a qubit spectra reflecting the photon number distribution in the cavity. In the cavity drive field, we use a different kind of states, such as thermal states, coherent states, and squeezed vacuum states. Thermal states are generated by amplifying the thermal noise at room temperature, and coherent states are generated by a microwave source at room temperature. They are led to the cavity through a series of attenuators to suppress the background noise. Squeezed vacuum states are generated by pumping a flux-driven JPA [31] at twice the JPA resonant frequency as

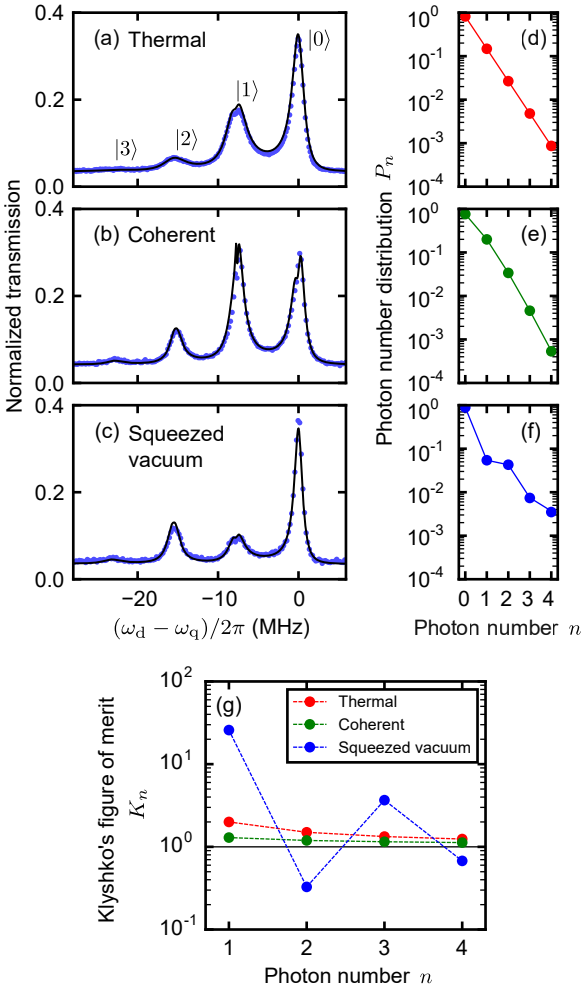

FIG. 3. (a)-(c) Qubit spectra reflecting the photon number distributions in the cavity. The cavity drive fields at frequency ω_s are in (a) thermal, (b) coherent, and (c) squeezed vacuum states, respectively. The average photon number in each state is set to about 0.2. Blue dots are the experimental data, and the black solid lines are the numerically calculated linear responses. (d)-(f) Photon number distributions determined from the fittings (dots). Solid lines are the photon number distributions calculated from the corresponding models. (g) Klyshko's figure of merit K_n evaluated for each drive.

shown in Fig. 1(a). The correlated photon pairs, generated from individual pump photons, result in an even-odd photon number oscillation in the photon number distribution. Note that the squeezed vacuum field propagating through the waveguide has a bandwidth broader than the cavity, and the photon pairs are generated symmetrically in frequency with respect to the center frequency of the squeezed vacuum in order to conserve energy.

First of all, we study the effect of the cavity probe field on qubit spectra. In Fig. 2(a), we plot the cavity transmission as a function of the cavity probe frequency ω_p and the qubit drive frequency ω_d. The red (blue) dots in Fig. 2(b) depict the cross-section at $\omega_p = \omega_c + \chi$ ($\omega_p = \omega_c - \chi$) in Fig. 2(a). Despite the absence of the cavity drive field at ω_s, we observe unexpected dips and peaks corresponding to single or double photon occupation in the cavity. Nevertheless, the numerical results obtained from the master equation taking into account the finite qubit drive and cavity probe power, reproduce these spectra very well (green lines) [30]. The excess dips in the spectrum at $\omega_p = \omega_c + \chi$ (cavity resonant frequency for the qubit in the ground state) are induced by the back-action of the cavity probe field on the cavity transmission. On the other hand, for $\omega_p = \omega_c - \chi$ (cavity resonant frequency for the qubit in the excited state), the back-action is minimal. Note that the small single-photon peak still remains due to the thermal background noise, corresponding to the average photon number $n_{th} = 0.04$ in the cavity. The black solid lines in Fig. 2(b) represent the numerical results within the linear response to the cavity probe field, which corresponds to the weak power limit of the probe [30]. The deviation of the linear response from the observed spectrum is smaller at $\omega_p = \omega_c - \chi$ than at $\omega_p = \omega_c + \chi$. For the measurements below, we fix the cavity probe frequency $\omega_p = \omega_c - \chi$ which does not influence the qubit spectra significantly and apply the linear-response analysis.

Qubit spectra obtained in the cavity driven by different states of microwave fields are shown in Figs. 3(a)-(c). The numerical calculations (black solid lines) reproduce well the experimental results (blue dots). Dots in Figs. 3(d)-(f) represent the photon number distributions in the cavity, determined from the numerical fits for the spectra. We compare them with the expectations based on simple models [30]. The red line in Fig. 3(d) is the distribution of a thermal state with the average photon number $n_{th} = 0.22$. The green line in Fig. 3(e) is the distribution of a thermal coherent state with $n_{th} = 0.04$ and the displacement parameter $\alpha = 0.49$. An even-odd photon number oscillation is observed both in the qubit spectrum and in the photon number distribution for the squeezed vacuum state [Figs. 3(c) and (f)]. The blue line in Fig. 3(f) is the distribution of a squeezed vacuum state with the squeezing parameter $r = 0.54$ and the loss ratio $l = 0.42$. This corresponds to a 2.1-dB squeezed state. Note that the determined photon number distributions have much less weights for larger n than the apparent peak area ratio in the qubit spectra. This is because the qubit excitation rate and the cavity decay rate are larger than the qubit decay rate. In the steady-state measurement, once the qubit is excited in the presence of the cavity photons ($n \geq 1$), the photons leave the cavity rapidly and the population accumulates in the state $|e, 0\rangle$. Therefore, the cavity transmission signal conditioned on the qubit excited state is enhanced.

To verify the nonclassicality of the photon number distribution under the squeezed drive, we evaluate Klyshko's figures of merit $K_n = \frac{(n+1)P_{n-1}P_{n+1}}{nP_n{}^2}$ ($n = 1, 2, \cdots$) [26]

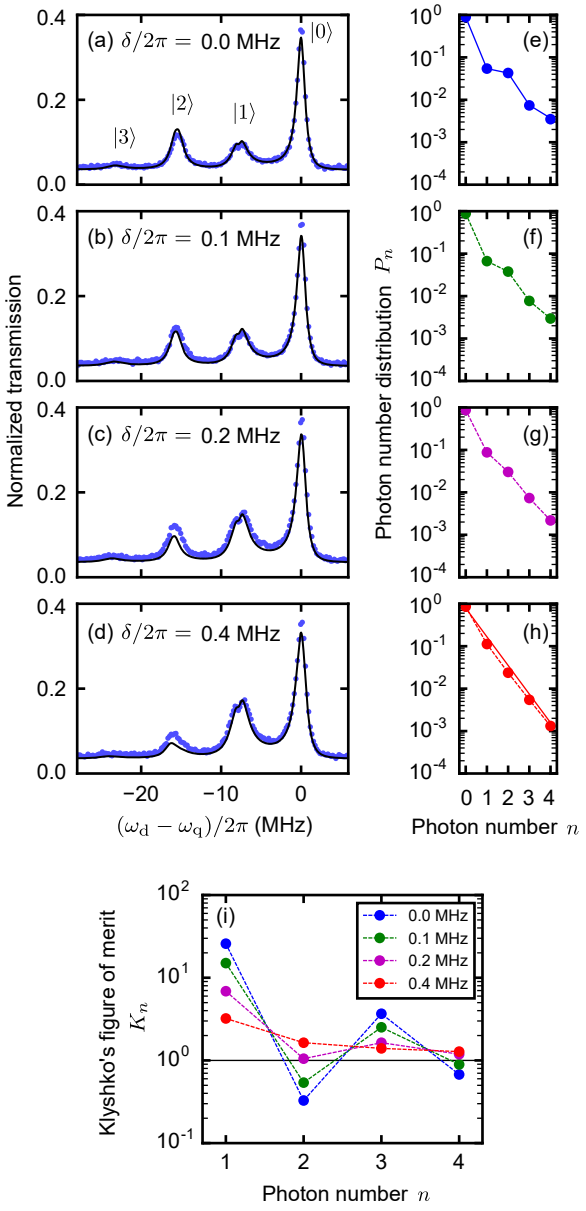

FIG. 4. (a)-(d) Squeezed-drive-frequency dependence of the qubit spectrum. $\delta = \omega_s - (\omega_c + \chi)$ is the detuning between the center frequency ω_s of the squeezed vacuum field and the cavity resonant frequency $\omega_c + \chi$. Blue dots are the experimental results, and black solid lines are the numerical calculations. (e)-(h) Photon number distributions determined from the fittings (dots and dashed lines). Solid lines in (e) and (h) are the photon number distributions calculated from the corresponding models. (i) Klyshko's figure of merit K_n evaluated for each detuning δ.

shown in Fig. 3(g). A set of K_n gives a nonclassicality criterion which can be calculated with the photon number distribution alone. If any of K_n is less than unity, the state is determined to be nonclassical. As shown in Fig. 3(g), K_n is below unity for $n = 2$ and 4 under the squeezed drive. Thus, the photon number distribution fulfills Klyshko's criterion for nonclassicality. In contrast, all the values of K_n up to 4 are found to be larger than unity for the coherent and the thermal drives.

Finally, we study the squeezed-drive-frequency dependence of the qubit spectrum as shown in Figs. 4(a)-(d). When the detuning δ between the center frequency ω_s of the broadband squeezed vacuum and the cavity resonant frequency $\omega_c + \chi$ is zero, both photons in a pair are injected into the cavity with a high and identical probability, so that the even-odd photon number oscillation is conserved. When the detuning is increased, however, the injection probabilities of the photon pairs are asymmetrically biased, and the photon number oscillation is weakened. In the large detuning limit, the cavity state becomes a thermal state. This can be understood from the fact that a two-mode squeezed vacuum state is reduced to a thermal state after tracing out one of the modes. In Fig. 4, we observe that the photon number oscillation is diminished as the detuning is increased. Eventually, the photon number distribution approaches the Boltzmann distribution of a thermal state with the average photon number $n_{\rm th} = 0.27$ [red solid line in Fig. 4(h)]. These observations indicate that a broadband squeezed vacuum has correlated photon pairs in frequency space. Klyshko's figures of merit plotted in Fig. 4(i) show that the nonclassicality is reduced as the detuning is increased and that the cavity state becomes a classical state, i.e., $K_n > 1$ for any photon number n.

In conclusion, we developed a circuit-QED scheme to characterize a microwave squeezed vacuum in the Fock basis. By analyzing the qubit spectrum in a cavity driven continuously by a squeezed vacuum, we determined the photon number distribution, which is associated with the squeezed vacuum in a propagating mode according to the input-output relation. Most importantly, the distribution fulfills Klyshko's criterion for nonclassicality.

We acknowledge the fruitful discussion with K. Wakui. This work was supported in part by the Project for Developing Innovation System of MEXT, ALPS, JSPS KAKENHI (No. 16K05497 and 26220601), and JST ERATO (Grant No. JPMJER1601).

[1] M. H. Devoret and R. J. Schoelkopf, Science **339**, 1169 (2013).
[2] A. Blais, R.-S. Huang, A. Wallraff, S. M. Girvin, and R. J. Schoelkopf, Phys. Rev. A **69**, 062320 (2004).
[3] P. D. Drummond and Z. Ficek, *Quantum Squeezing*, Vol. 27 (Springer Science & Business Media, 2013).
[4] R. Movshovich, B. Yurke, P. G. Kaminsky, A. D. Smith, A. H. Silver, R. W. Simon, and M. V. Schneider, Phys. Rev. Lett. **65**, 1419 (1990).
[5] M. Castellanos-Beltran, K. Irwin, G. Hilton, L. Vale, and K. Lehnert, Nature Phys. **4**, 929 (2008).

[6] F. Mallet, M. A. Castellanos-Beltran, H. S. Ku, S. Glancy, E. Knill, K. D. Irwin, G. C. Hilton, L. R. Vale, and K. W. Lehnert, Phys. Rev. Lett. **106**, 220502 (2011).

[7] E. P. Menzel, R. Di Candia, F. Deppe, P. Eder, L. Zhong, M. Ihmig, M. Haeberlein, A. Baust, E. Hoffmann, D. Ballester, K. Inomata, T. Yamamoto, Y. Nakamura, E. Solano, A. Marx, and R. Gross, Phys. Rev. Lett. **109**, 250502 (2012).

[8] L. Zhong, E. P. Menzel, R. Di Candia, P. Eder, M. Ihmig, A. Baust, M. Haeberlein, E. Hoffmann, K. Inomata, T. Yamamoto, Y. Nakamura, E. Solano, F. Deppe, A. Marx, and R. Gross, New J. Phys. **15**, 125013 (2013).

[9] C. M. Wilson, G. Johansson, A. Pourkabirian, M. Simoen, J. R. Johansson, T. Duty, F. Nori, and P. Delsing, Nature **479**, 376 (2011).

[10] C. Eichler, D. Bozyigit, C. Lang, M. Baur, L. Steffen, J. M. Fink, S. Filipp, and A. Wallraff, Phys. Rev. Lett. **107**, 113601 (2011).

[11] N. Bergeal, F. Schackert, L. Frunzio, and M. H. Devoret, Phys. Rev. Lett. **108**, 123902 (2012).

[12] E. Flurin, N. Roch, F. Mallet, M. H. Devoret, and B. Huard, Phys. Rev. Lett. **109**, 183901 (2012).

[13] C. Macklin, K. O'Brien, D. Hover, M. E. Schwartz, V. Bolkhovsky, X. Zhang, W. D. Oliver, and I. Siddiqi, Science **350**, 307 (2015).

[14] K. W. Murch, S. J. Weber, K. M. Beck, E. Ginossar, and I. Siddiqi, Nature **499**, 62 (2013).

[15] D. M. Toyli, A. W. Eddins, S. Boutin, S. Puri, D. Hover, V. Bolkhovsky, W. D. Oliver, A. Blais, and I. Siddiqi, Phys. Rev. X **6**, 031004 (2016).

[16] A. Bienfait, P. Campagne-Ibarcq, A. Holm-Kiilerich, X. Zhou, S. Probst, J. J. Pla, T. Schenkel, D. Vion, D. Esteve, J. J. L. Morton, K. Moelmer, and P. Bertet, arXiv:1610.03329 (2016).

[17] W. Schleich and J. Wheeler, Nature **326**, 574 (1987).

[18] E. Waks, B. C. Sanders, E. Diamanti, and Y. Yamamoto, Phys. Rev. A **73**, 033814 (2006).

[19] K. Wakui, Y. Eto, H. Benichi, S. Izumi, T. Yanagida, K. Ema, T. Numata, D. Fukuda, M. Takeoka, and M. Sasaki, Sci. Rep. **4**, 4535 (2014).

[20] Y.-F. Chen, D. Hover, S. Sendelbach, L. Maurer, S. T. Merkel, E. J. Pritchett, F. K. Wilhelm, and R. McDermott, Phys. Rev. Lett **107**, 217401 (2011).

[21] K. Inomata, Z. Lin, K. Koshino, W. D. Oliver, J. S. Tsai, T. Yamamoto, and Y. Nakamura, Nature Commun. **7**, 12303 (2016).

[22] A. Narla, S. Shankar, M. Hatridge, Z. Leghtas, K. M. Sliwa, E. Zalys-Geller, S. O. Mundhada, W. Pfaff, L. Frunzio, R. J. Schoelkopf, and M. H. Devoret, Phys. Rev. X **6**, 031036 (2016).

[23] D. I. Schuster, A. A. Houck, J. A. Schreier, A. Wallraff, J. M. Gambetta, A. Blais, L. Frunzio, J. Majer, B. Johnson, M. H. Devoret, S. H. Girvin, and R. J. Schoelkopf, Nature **445**, 515 (2007).

[24] B. Suri, Z. K. Keane, L. S. Bishop, S. Novikov, F. C. Wellstood, and B. S. Palmer, Phys. Rev. A **92**, 063801 (2015).

[25] J. Gambetta, A. Blais, D. I. Schuster, A. Wallraff, L. Frunzio, J. Majer, M. H. Devoret, S. M. Girvin, and R. J. Schoelkopf, Phys. Rev. A **74**, 042318 (2006).

[26] D. N. Klyshko, Phys. Lett. A **213**, 7 (1996).

[27] A. A. Clerk, M. H. Devoret, S. M. Girvin, F. Marquardt, and R. J. Schoelkopf, Rev. Mod. Phys. **82**, 1155 (2010).

[28] M. Hofheinz, H. Wang, M. Ansmann, R. C. Bialczak, E. Lucero, M. Neeley, A. D. O'Connell, D. Sank, J. Wenner, J. M. Martinis, and A. N. Cleland, Nature **459**, 546 (2009).

[29] B. Vlastakis, G. Kirchmair, Z. Leghtas, S. E. Nigg, L. Frunzio, S. M. Girvin, M. Mirrahimi, M. H. Devoret, and R. J. Schoelkopf, Science **342**, 607 (2013).

[30] See accompanying supplementary materials for details, which includes Refs. [32, 33].

[31] T. Yamamoto, K. Inomata, M. Watanabe, K. Matsuba, T. Miyazaki, W. Oliver, Y. Nakamura, and J. Tsai, Appl. Phys. Lett. **93**, 042510 (2008).

[32] A. A. Clerk and D. W. Utami, Phys. Rev. A **75**, 042302 (2007).

[33] B. Suri, Z. K. Keane, R. Ruskov, L. S. Bishop, C. Tahan, S. Novikov, J. E. Robinson, F. C. Wellstood, and B. S. Palmer, New J. of Phys. **15**, 125007 (2013).